Available online at www.sciencedirect.com
ScienceDirect
C. R. Physique 9 (2008) 885–901
COMPTES RENDUS PHYSIQUE
http://france.elsevier.com/direct/COMREN/

Recent advances in quantum dot physics / Nouveaux développements dans la physique des boîtes quantiques

Optical probing of the spin state of a single magnetic atom in a quantum dot

Lucien Besombes *, Yoan Leger, Hervé Boukari, Laurent Maingault, David Ferrand, Joël Cibert, Henri Mariette

CEA-CNRS group "Nanophysique et Semiconducteurs", Néel Institute, CNRS and University J. Fourier, 25, avenue des Martyrs, 38042 Grenoble cedex 9, France

Available online 14 November 2008

Abstract

The magnetic state of a single magnetic ion (Mn^{2+}) embedded in an individual quantum dot is optically probed using microspectroscopy. The fine structure of a confined exciton in the exchange field of a single Mn^{2+} ion ($S = 5/2$) is analyzed in detail. The exciton–Mn^{2+} exchange interaction shifts the energy of the exciton depending on the Mn^{2+} spin component and six emission lines are observed at zero magnetic field. The QD exciton emission is then a direct probe of the Mn spin state. The limiting factors of such detection are then presented: they are mainly due to the influence of geometrical effects such as the anisotropic strain distribution into the QD and its shape anisotropy. In the last part, we show how we can manipulate and understand quantitatively the interaction between the single Mn spin and a confined carrier by controlling the charge state of a quantum dot ($0, \pm 1$ electron) with an electrostatic (and optical) gate. This opens the way to an electrical or optical control of the magnetic properties of a single atom. ***To cite this article: L. Besombes et al., C. R. Physique 9 (2008).***

Résumé

Mesure optique de l'état de spin d'un atome magnétique dans une boite quantique. L'état magnétique d'un ion magnétique unique (Mn^{2+}) inséré dans une boîte quantique individuel est sondé optiquement par micro-spectroscopie. La structure fine de l'exciton confiné dans le champ d'échange de l'ion unique Mn^{2+} ($S = 5/2$) est analysée en détails. L'interaction d'échange exciton–Mn^{2+} induit un changement d'énergie de l'exciton qui dépend de la composante de spin du Mn^{2+}, et six raies d'émission sont observées à champ magnétique nul. Ainsi, l'émission excitonique de la boîte quantique est une sonde directe de l'état de spin du manganèse. Les facteurs limitant d'une telle détection sont présentés : ils sont principalement dus à l'influence des effets géométriques tels que la distribution inhomogène des contraintes dans la boîte et la forme anisotrope de celle-ci. Dans une dernière partie, nous montrons comment on peut manipuler et comprendre quantitativement l'interaction entre un spin de manganèse unique et un porteur de charge confiné, en contrôlant l'état de charge de la boîte ($0, \pm 1$ électron) optiquement ou par une tension électrostatique. Ceci ouvre la voie à un contrôle électrique (ou optique) des propriétés magnétiques d'un atome unique. ***Pour citer cet article : L. Besombes et al., C. R. Physique 9 (2008).***

Keywords: Quantum dots; Optical properties; Magnetic impurities

* Corresponding author.
E-mail address: lucien.besombes@grenoble.cnrs.fr (L. Besombes).

1631-0705/$ – see front matter
doi:10.1016/j.crhy.2008.10.013

Mots-clés : Boîtes quantiques ; Propriétés optiques ; Impuretés magnétiques

1. Introduction

As the size of magneto-electronic devices scales down, it becomes increasingly important to understand the properties of a single magnetic atom in a solid state environment [1–4,6]. Atomic scale surface probes have been successfully used in this regard [1–3]. More recently, optical probing of both magnetic [4,5] and non-magnetic [7] atoms in semiconductors has been demonstrated. Magnetically doped semiconductors have been used in the fabrication of electrically active devices that control the magnetic properties like transition temperature and coercitive field [8–10]. In these devices a macroscopic number of magnetic atoms was manipulated. We will present here electrically active devices that control the charge state of an individual II-VI quantum dot (QD) doped with a single Mn atom. Single dot micro-photoluminescence measurements reveal that the magnetic anisotropy and spin configuration of the single Mn atom are very different depending on the charge state of the dot, which can be 0, or $\pm$1e. Thus, these devices are able to tune the magnetic properties of a single Mn atom embedded in a QD which represents a first step in the implementation of several proposals of electrical control of the magnetism in Mn-doped quantum dots [11,14,12,13].

Quantum dots doped with magnetic atoms and filled with a tunable number of carriers can behave like tunable nanomagnets. Indeed, as it has been theoretically shown, the parity of the number of confined carriers can drastically change the magnetic properties of the localized magnetic moments [12–16].

In a magnetic QD, the sp-d interaction takes place with a single carrier or a single electron–hole pair. However, besides effects related to the carriers–Mn-ions exchange interaction such as giant Faraday rotation and strong Zeeman shift, it was found that even a small content of Mn introduced in a II-VI semiconductor material can strongly suppress photoluminescence if the energy gap E_g exceeds the energy of the Mn internal transition. This strongly limits the study of individual diluted magnetic semiconductor quantum dots [17]. The first studies of individual quantum dots doped with Mn atoms were reported by Maksimov et al. [18]. They studied CdMnTe QDs inserted in CdMgTe barriers in which the optical transition energies are lower than the energy of the internal transition of the Mn atom. This suppresses the non-radiative losses due to the transfer of confined carriers to the Mn energy levels. This system allowed the observation of the formation of a quasi zero-dimensional magnetic polaron. Moreover, the broadening of the emission lines caused by the magnetic fluctuations in the environment of the recombining electron hole pair was controlled by an external magnetic field.

Another way to reduce the non-radiative losses was to introduce the magnetic atoms in the quantum dots barriers. This has been realized for CdSe dots embedded in ZnMnSe barriers by Seufert et al. [19]. In this system, the interaction between the confined exciton and the magnetic ions is due to the spread of the wave function in the barriers and to a small diffusion of the magnetic atoms in the quantum dots. In these diluted magnetic semiconductor (DMS) structures, the response time of the paramagnetic Mn spin was extracted from the transient spectral shift of the photoluminescence caused by the dynamical spin alignment of magnetic ions incorporated into the crystal matrix. The formation of a ferromagnetically aligned spin complex was demonstrated to be surprisingly stable as compared to bulk magnetic polaron [20,21], even at elevated temperature and high magnetic fields. The photoluminescence of a single electron–hole pair confined in one magnetic QD, which sensitively depends on the alignment of the magnetic ions spins, allowed one to measure the statistical fluctuation of the magnetization on the nanometer scale. Quantitative access to statistical magnetic fluctuations was obtained by analyzing the linewidth broadening of the single dot emission. This all optical technique allowed to address a magnetic moment of about $100\mu_B$ and to resolve changes in the order of a few μ_B [24,22,23].

A huge effort has also been made to incorporate magnetic ions in chemically synthesized II-VI nanocrystals [25]. The incorporation of the magnetic impurities is strongly dependent on the growth conditions and controlled by the adsorption of impurities on the nanocrystal surface during growth [26]. The doping of nanocrystals with magnetic impurities also led to interesting magneto-optical properties [27] but once again, in these highly confined systems, the transfer of confined carriers to the Mn electronic levels strongly reduces their quantum efficiency and prevents the optical study of individual Mn-doped nanocrystals. However, by looking to magnetic circular dichroism (MCD) absorption spectra it is possible to observe a giant excitonic Zeeman splitting and to deduce directly the sp-d exchange interaction [28].

CdTe/ZnTe self assembled QDs usually present an emission energy below the internal transition of the Mn atom. The incorporation of magnetic atoms is then possible without losing the good optical properties of these QDs. Up to now, however, all the experimental studies on these diluted magnetic QDs were focused on the interaction of a single carrier spin with its paramagnetic environment (large number of magnetic atoms) [29]. We will see that CdTe/ZnTe quantum dot structures doped with a low density of Mn atoms allow us to control optically the spin states of a single magnetic ion interacting with a single electron–hole pair or a single carrier.

2. II-VI diluted magnetic semiconductors QDs

Carrier–Mn coupling was mostly studied in bulk DMS made of II-VI semiconductors in which Mn impurities were introduced (see the review papers [30,31]). These semiconductors are formed with a cation from column II (Zn, Cd or Hg) and an anion from column VI (Te, Se, S and more recently even O). These compounds assume the zinc-blende structure or, for the most ionic ones, the closely related wurtzite structure. Manganese impurities have the d^5 electronic configuration and substitute the cations up to 100%. An important point is that Mn substitutes the column-II cation as an isoelectronic impurity – by contrast to the acceptor character observed in GaAs and similar III-Vs [32,33]. The Mn ground state is 6S (or 6A1 in cubic or hexagonal symmetry), introducing localized, isotropic spins with $S = 5/2$. If not interacting, these localized spins follow Maxwell–Boltzmann statistics, resulting in a magnetization M induced by an applied field H at temperature T given by a Brillouin function. Optical spectroscopy around the bandgap reveals the so-called "giant Zeeman effect", with a spin splitting proportional to the Mn magnetization [35]. Several studies have demonstrated this proportionality and measured the strength of the coupling [36]. Magneto-optical spectroscopy is now a very sensitive method for measuring locally the magnetization of the Mn system. Altogether, this excellent knowledge of the magnetic properties in (electrically) undoped II-VI DMSs, and of the coupling between the localized spins and the conduction/valence band, constitutes a very firm basis for the further studies described below.

The CdTe/ZnTe QDs samples used in this study are grown by Atomic Layer Epitaxy (ALE) with a deposition of 6 monolayers of CdTe on a ZnTe buffer. Single Mn atoms are introduced in CdTe/ZnTe QDs during their growth adjusting the density of Mn atoms to be roughly equal to the density of QDs [34]. The QDs are then capped with a ZnTe barrier.

3. Confined carriers-Mn exchange interaction

Micro-spectroscopy was used to study the magneto-optical properties of individual CdTe/ZnTe QDs. The low temperature (5 K) photoluminescence (PL) of single QDs is excited with the 514.5 nm line of an argon laser or a tunable dye laser and collected through a large numerical-aperture objective and aluminium shadow masks with 0.5–1.0 m apertures. The experiments are carried out in the backward geometry with the propagation direction of the incident and emitted light parallel to the [001] growth axis. Superconductive coils are used to apply a magnetic field up to 11 T in the Voigt or Faraday configuration. The PL is then dispersed by a 2 m double monochromator and detected by a nitrogen-cooled Si charged-coupled device camera or a Si avalanche photodiode.

In Fig. 1, PL spectra of an individual Mn-doped QD are compared to those of a non-magnetic CdTe/ZnTe reference sample. In non-magnetic samples, narrow PL peaks (limited by the spectrometer resolution of about 50 μeV) can be resolved, each attributed to the recombination of a single electron–hole pair in a single QD. The emission of neutral QDs is split by the e–h exchange interaction and usually a linearly polarized doublet is observed [39]. On the other hand, most of the individual emission peaks of magnetic single QDs are characterized by a rather large linewidth of about 0.5 meV. For some of these QDs, a fine structure can be resolved and six emission lines are clearly observed at zero magnetic field. The measured splitting changes from dot to dot. This fine structure splitting as well as the broadening is obviously related to the influence of the magnetic ions located within the spatial extent of the exciton wave function. The broadening observed in magnetic QDs has been attributed by Bacher et al. to the magnetic fluctuations of the spin projection of a *large number* of Mn spins interacting with the confined exciton [24]. In the low concentration Mn-doped samples, the observation of a fine structure shows that the QD exciton interacts with a single Mn spin. In time-averaged experiments, the statistical fluctuations of a single Mn spin ($S = 5/2$) can be described in terms of populations of its six spin states quantized along the direction normal to the QD plane. The exchange interaction of the confined exciton with the Mn atom shifts its energy depending on the Mn spin projection, resulting in the observation of six emission lines.

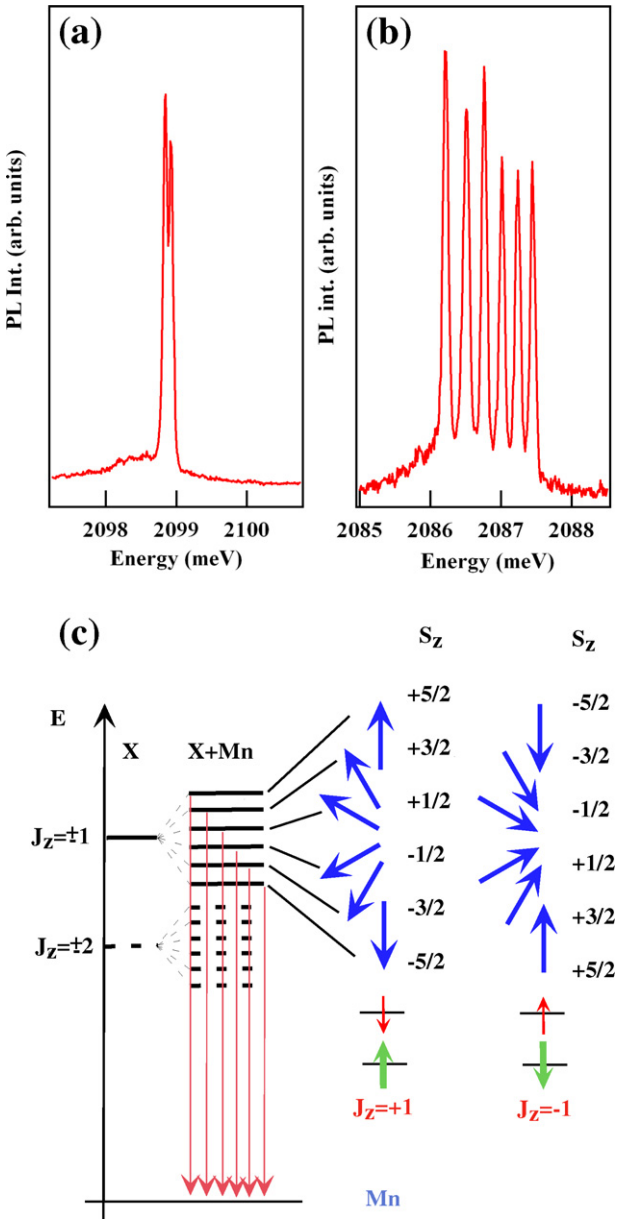

Fig. 1. (Color online.) Low temperature ($T = 5$ K) PL spectra obtained at $B = 0$ T for an individual CdTe/ZnTe QD (a) and a Mn-doped QD (b). (c) Scheme of the energy levels of the Mn–exciton coupled system at zero magnetic field. The exciton–Mn exchange interaction shift the energy of the exciton depending on the S_z component of the Mn spin projection.

QDs doped with single Mn atoms were considered theoretically in the case of spherical nanocrystals with a strong confinement [27]. The eigenstates resulting from the exchange coupling between the exciton and the magnetic ion, were obtained by a combination of the electron, hole and Mn magnetic moments. In flat self-assembled QDs with a relatively weak confinement, the bi-axial strains in the plane of the QD lift the degeneracy of the hole spin projections (heavy-hole/light hole splitting). In a first approximation, this system can be described by a heavy-hole exciton confined in a symmetric QD, in interaction with the six spin projections of the manganese ion [37]. The spin interaction part of the Hamiltonian of is given by:

$$H_{\text{int}} = I_{\text{e}}\sigma \cdot S + I_{\text{h}} j \cdot S + I_{\text{eh}}\sigma \cdot j \tag{1}$$

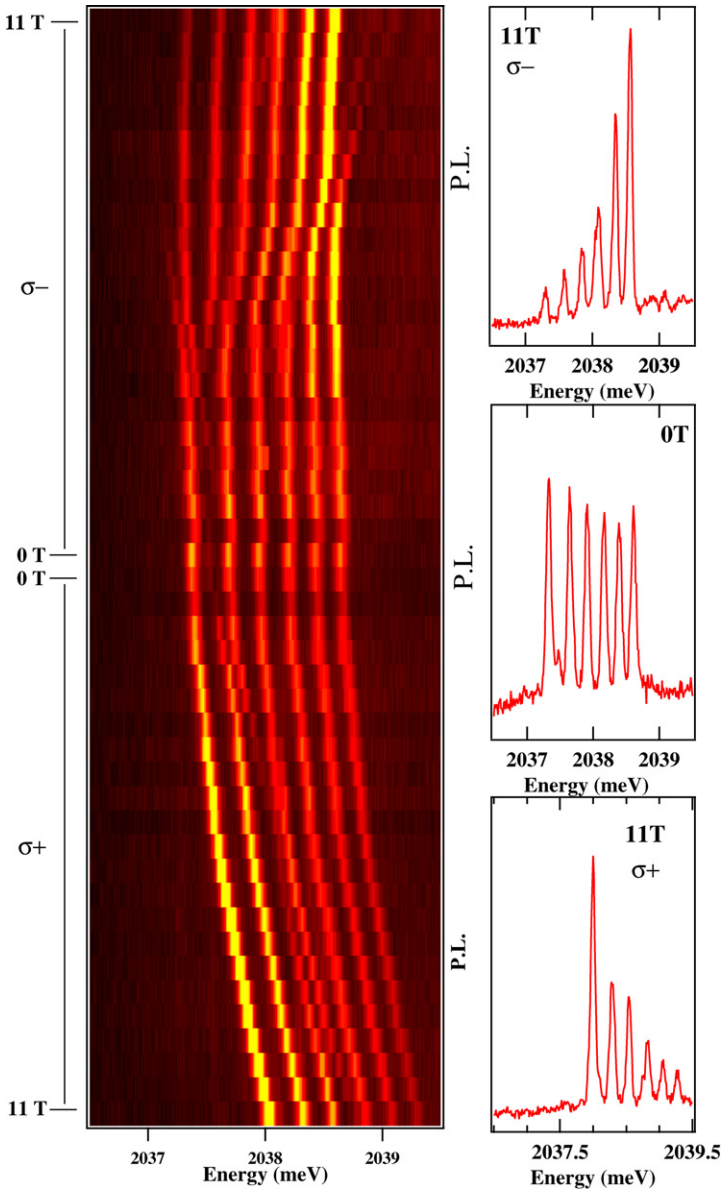

Fig. 2. (Color online.) Magnetic field dependence of the emission of a Mn-doped QD recorded in $\sigma+$ and $\sigma-$ polarisation. Anticrossing of the bright and dark states appears around 7 T in $\sigma-$ polarisation.

where I_e (I_h) is the Mn–electron (–hole) exchange integral, I_{eh} the electron–hole exchange interaction and σ (j, S) the magnetic moment of the electron (hole, Mn). The initial states of the optical transitions are obtained from the diagonalization of the spin Hamiltonian and Zeeman Hamiltonian in the subspace of the heavy hole exciton and Mn spin components $|\pm 1/2\rangle_e|\pm 3/2\rangle_h|S_z\rangle_{Mn}$, with $S_z = \pm 5/2$, $\pm 3/2$, $\pm 1/2$. Since the dipolar interaction operator does not affect the Mn d electrons, the final states involve only the Mn states $|S_z\rangle_{Mn}$ with the same spin component [4].

In this framework, at zero magnetic field, the QD emission presents a fine structure composed of six doubly degenerate transitions roughly equally spaced in energy. The lower energy bright states, $|+1/2\rangle_e|-3/2\rangle_h|+5/2\rangle_{Mn}$ and $|-1/2\rangle_e|+3/2\rangle_h|-5/2\rangle_{Mn}$ are characterized by an anti-ferromagnetic coupling between the hole and the Mn atom. The following states are associated with the Mn spin projections $S_z = \pm 3/2$, $\pm 1/2$ until the higher energy states $|-1/2\rangle_e|+3/2\rangle_h|+5/2\rangle_{Mn}$ and $|+1/2\rangle_e|-3/2\rangle_h|-5/2\rangle_{Mn}$ corresponding to ferromagnetically coupled hole and man-

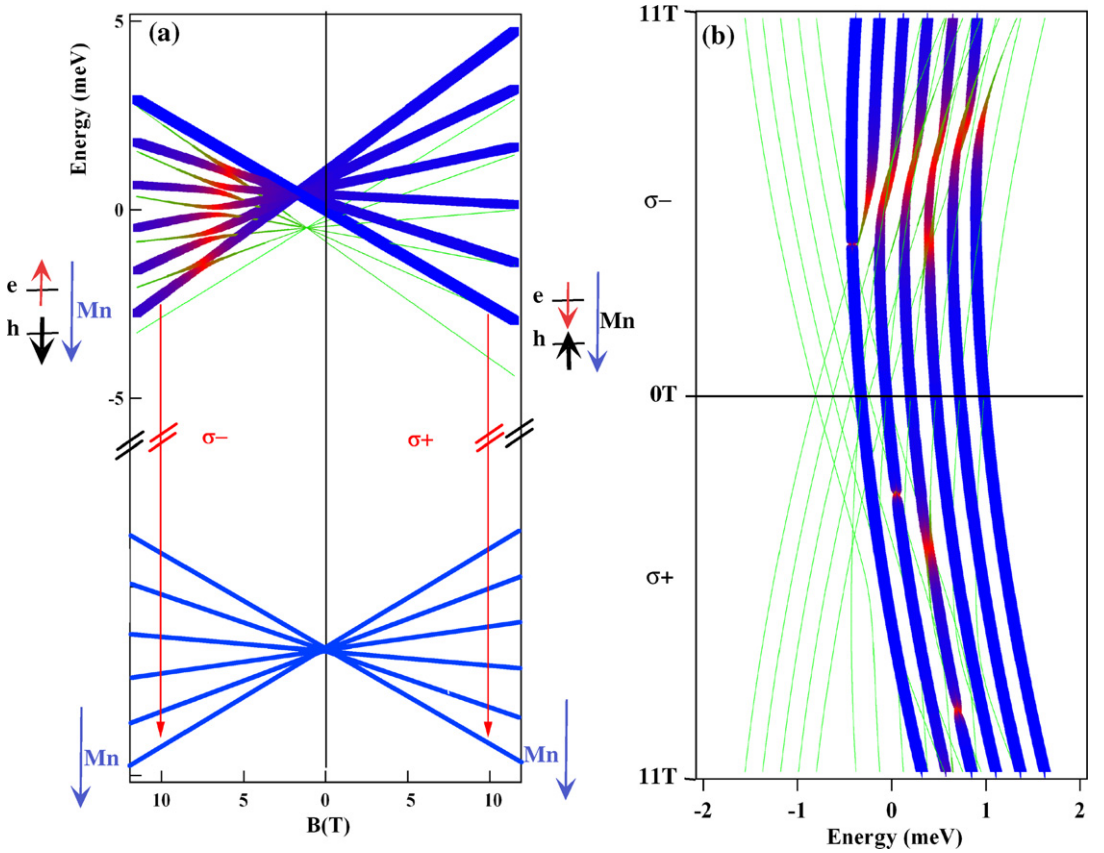

Fig. 3. (a) scheme of the energy levels of the initial and final state involved in the optical transitions of a quantum dot containing a Mn atom. (b) Modelization of the optical transition obtained from the diagonalization of an effective spin Hamiltonian including the e–h exchange interaction, the exciton–Mn exchange interaction, the Zeeman and the diamagnetic energies. The contribution of the dark states appears in green.

ganese. In this simple model the zero field splitting $\delta_{\mathrm{Mn}} = \frac{1}{2}(I_{\mathrm{e}} - 3I_{\mathrm{h}})$ depends only on the exchange integrals I_{e} and I_{h} and is thus related to the position of the Mn atom within the exciton wave function.

When an external magnetic field is applied in the Faraday geometry (Fig. 2), each PL peak is further split and twelve lines are observed, six in each circular polarization. As presented in Fig. 3, the Zeeman effect of the Mn states is identical in the initial and final states of the optical transitions then the six lines in a given polarization follow the Zeeman and diamagnetic shift of the exciton, as in a non-magnetic QD. The parallel evolution of six lines is perturbed around 7 T in $\sigma-$ polarization by anti-crossings observed for five of the lines. In addition, as the magnetic field increases, one line in each circular polarization increases in intensity and progressively dominates the others.

The electron–Mn part of the interaction Hamiltonian $I_{\mathrm{e}}(\sigma \cdot S)$ couples the dark ($J_z = \pm 2$) and bright ($J_z = \pm 1$) heavy hole exciton states. This coupling corresponds to a simultaneous electron and Mn spin flip changing a bright exciton into a dark exciton. Because of the strain induced splitting of light hole and heavy hole levels, a similar Mn–hole spin flip scattering is not allowed. The electron–Mn spin flip is enhanced as the corresponding levels of bright and dark excitons are brought into coincidence by the Zeeman effect. An anti-crossing is observed around 7 T for five of the bright states in $\sigma-$ polarization (experiment: Fig. 2 and theory: Fig. 3). It induces a transfer of oscillator strength to the dark states. In agreement with the experimental results, in the calculations the lower energy state in $\sigma-$ polarization ($|+1/2\rangle_{\mathrm{e}}|-3/2\rangle_{\mathrm{h}}|+5/2\rangle_{\mathrm{Mn}}$) does not present any anti-crossing. In this spin configuration, both the electron and the Mn atom have maximum spin projection and a spin flip is not possible.

The minimum energy splitting at the anti-crossing is directly related to the electron–Mn exchange integral I_{e}. For instance, the splitting measured for the higher energy line in $\sigma-$ polarisation (Fig. 2), $\Delta E = 150$ μeV gives $I_{\mathrm{e}} \approx 70$ μeV. From the overall splitting measured at zero field (1.3 meV) and with this value of I_{e}, we obtain $I_{\mathrm{h}} \approx -150$ μeV. These values are in good agreement with values estimated from a modeling of the QD confinement by a

square quantum well in the growth direction and a truncated parabolic potential in the QD plane. With a quantum well thickness $L_z = 3$ nm and a Gaussian wave function characterized by an in-plane localization parameter $\xi = 5$ nm we obtain $I_e \approx 65$ μeV for a Mn atom placed at the center of the QD.

However, the ratio of the exchange integral, $(3I_h)/I_e \approx -6$ for the QD presented in Fig. 2, does not directly reflects the ratio of the sp-d exchange constants $\beta/\alpha \approx -4$ measured in bulk CdMnTe alloys [30]. Such deviation likely comes from the difference in the electron–Mn and hole–Mn overlap expected from the difference in the electron and hole confinement lengths, but it could also be due to a change of the exchange parameters induced by the confinement [40]. A dispersion of the zero field energy splitting observed from dot to dot is then due to a variation of the Mn–exciton overlap for different QDs. However, the spin Hamiltonian (1) does not reproduce the observed non-uniform zero field splitting between consecutive lines (Fig. 1(b)). As we will see in the following, a more accurate model has to take into account the full valence band structure and the heavy-hole light-hole mixing.

4. Geometrical effects on the optical properties of a QD doped with a single magnetic atom

4.1. Influence of an anisotropic strain distribution

Several phenomena can lead to the mixing of light and heavy holes in QDs. First, the symmetry reduction due to the confinement geometry of the dot has to be considered. In this case, a hole band mixing appears through the non-diagonal terms of the Luttinger–Kohn Hamiltonian. This mixing is responsible for the linear polarization rate observed in strongly confined quantum wires [52]. A large wave function anisotropy is needed to reproduce the observed linear polarization [53]. Such anisotropy can only be obtained in a very elongated confining potential for the holes with large barriers. This is inconsistent with the observation of huge linear polarization rates in shallow CdTe/ZnTe QDs presenting a quite weak in-plane asymmetry as revealed by AFM measurements [34]. Another origin of hh–lh mixing is the coupling of the X and Y valence band states produced by the microscopic arrangement of chemical bonds at hetero-interfaces [54]. This contribution is expected to be weak in flat self assembled QDs with almost symmetric interfaces.

As we will see in the following, an efficient mixing can arise from the anisotropic relaxation of strains in the QDs plane. Influence of strains on hole states has been intensively studied in quantum wells. Two main effects have been demonstrated, namely the variation of the gap due to hydrostatic strains and the hh–lh degeneracy lift due to biaxial strains. We will show that in QDs the strain distribution can also be responsible for a strong lh–hh mixing. This mixing has striking effects on the hole spin anisotropy.

In bulk semiconductor, the spin orbit interaction is responsible for a splitting of the hole states. We only consider here the lowest energy holes with angular momentum $j = 3/2$. These $|j, j_z\rangle$ states can be simply defined using orbital (X, Y, Z) and spin $(\uparrow, \downarrow)$ eigenvectors:

$$
\begin{aligned}
|3/2, +3/2\rangle &= -\uparrow \frac{X + iY}{\sqrt{2}} \\
|3/2, +1/2\rangle &= \sqrt{\frac{2}{3}}\uparrow Z - \downarrow \frac{X + iY}{\sqrt{6}} \\
|3/2, -1/2\rangle &= \sqrt{\frac{2}{3}}\downarrow Z + \uparrow \frac{X - iY}{\sqrt{6}} \\
|3/2, -3/2\rangle &= \downarrow \frac{X - iY}{\sqrt{2}}
\end{aligned}
\tag{2}
$$

Using these notations, the Bir–Pikus Hamiltonian describing the influence of the strain on the valence band structure is written:

$$
H_{BP} = -a_v \sum_i \varepsilon_{ii} - b \sum_i \varepsilon_{ii}\left(j_i^2 - 1/3 j^2\right) - \frac{2d}{\sqrt{3}}\left(\varepsilon_{xy}\frac{j_x j_y + j_y j_x}{2} + \text{c.p.}\right) \tag{3}
$$

where the abbreviation c.p. is used for circular permutation over x, y and z corresponding to the crystal axes. The matrices of the angular momentum operator $\vec{j}$ can be found in Ref. [47]. ε_{ij} denotes the ij component of the strain

tensor and a_v, b and d are the deformation potentials for the valence band. Using the hole formalism, J. Allègre et al. found $a_v = 0.91$ eV, $b = 0.99$ eV and $d = 2.76$ eV for CdTe [49].

While growing CdTe on ZnTe, CdTe is compressed in the growth plane and distended in the growth direction. CdTe QDs form by deformation of a two dimensional layer induced by strain relaxation. In this formation mechanism, both elastic and inelastic strain relaxations are involved and one expect each QD to probe a different local in-plane strain distribution. When studying a particular QD, one has to consider a particular set of values for ε_{ij}. In the following, we will mainly consider the effects of strain anisotropy in the growth plane and describe the strain on each QD by an average value of ε_{xy} and $\varepsilon_{xx} - \varepsilon_{yy}$. An non-zero value of the volume average ε_{ij} can result from a local deformation of the lattice induced by neighbors QDs or dislocations. In this approximation, the Bir and Pikus Hamiltonian is reduced to a block-diagonal matrix in the $(+3/2, -1/2, +1/2, -3/2)$ basis:

$$H_{\mathrm{BP}} = \begin{pmatrix} P+Q & R & & \\ R^{\dagger} & P-Q & & \\ & & P-Q & R \\ & & R^{\dagger} & P+Q \end{pmatrix} \tag{4}$$

with,

$$P = a_v \sum_i \varepsilon_{ii} \tag{5}$$

$$Q = b\left(\frac{\varepsilon_{xx} + \varepsilon_{yy}}{2} - \varepsilon_{zz}\right)$$

$$R = id\varepsilon_{xy} - b\frac{\sqrt{3}}{2}(\varepsilon_{xx} - \varepsilon_{yy})$$

Using the hh band as the origin of the energies in the valence band, the strain Hamiltonian can be rewritten as:

$$H_{\mathrm{BP}} = \begin{pmatrix} 0 & \rho_s e^{-2i\theta'_s} & & \\ \rho_s e^{2i\theta'_s} & \Delta_{\mathrm{lh}} & & \\ & & \Delta_{\mathrm{lh}} & \rho_s e^{-2i\theta'_s} \\ & & \rho_s e^{2i\theta'_s} & 0 \end{pmatrix} \tag{6}$$

This notation allows us to introduce useful parameters to describe the strain effects, namely the light-heavy hole splitting Δ_{lh}, the strain coupling amplitude ρ_s and the strain induced anisotropy axis in the QD plane defined by the angle θ'_s with respect to the x (100) axis. In the following, we will define angles relatively to the (110) axis corresponding to the cleaved edge of the sample. We thus introduce the new angle $\theta_s = \theta'_s - 45°$. Because of the strained induced VBM described by the Hamiltonian (6), the general form for the lowest energy hole states is:

$$\left|\varphi_{\mathrm{h}}^{\pm}\right\rangle \propto \chi_{\mathrm{hh}}(\vec{r}\,)|\pm 3/2\rangle - \frac{w_{\mathrm{lh}}}{w_{\mathrm{hh}}}\chi_{\mathrm{lh}}(\vec{r}\,)|\mp 1/2\rangle \tag{7}$$

where $w_{\mathrm{lh(hh)}}$ is the probability for the hole to be light (heavy) and $\chi_{\mathrm{lh(hh)}}(\vec{r}\,)$ its envelope function.

Considering now single Mn-doped QDs, the sp-d exchange interactions between the confined carriers and the single Mn atom are responsible for a peculiar fine structure of the emission [4]. It has been demonstrated that the hole–Mn spin interaction is of prime importance in this fine structure, because of its energy range and above all because of the spin anisotropy of the hole [45,46]. It appears clearly that a valence band mixing will have dramatic consequences on the emission fine structures of Mn doped QDs. In the heavy hole approximation, a hole acts on the Mn spin as an effective magnetic field applied along the growth axis, lifting its spin degeneracy. If a mixing of heavy and light holes is introduced, one has to consider a system of coupled spins in which hole–Mn spin flips becomes possible.

One can find a signature of the valence band mixing in the emission spectra of neutral single Mn-doped QDs [47]. In a Mn-doped QD, the ground state of the exciton is composed of six bright energy levels and six dark energy levels resulting from the coupling of bright excitons and dark excitons with the six projections of the Mn spin. For a given exciton spin (± 1 or ± 2), the six Mn spin projection have different energies. In this system, the hole spin interacts with both the Mn spin and the electron spin. The effect of an increasing valence band mixing on the excitonic emission spectrum of a QD is presented on Fig. 4(a). Parameters are chosen to reproduce the features of QD5 emission spectrum plotted on Fig. 4(b): the e–Mn exchange integral $I_{\mathrm{e-Mn}}$ is set to 70 μeV; the splitting between bright and dark exciton

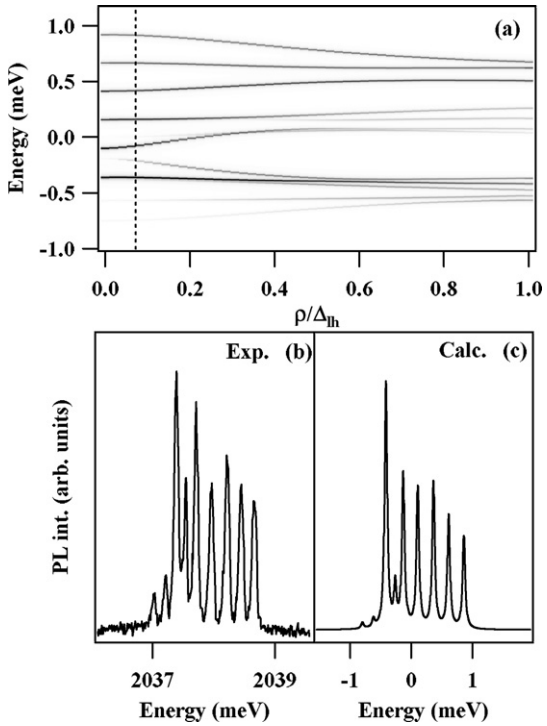

Fig. 4. (a) Dependence of the exciton–Mn energy spectrum on the strength of the valence band mixing $\rho/\Delta_{\mathrm{lh}}$. The dotted line corresponds to the situation of QD6 ($\rho/\Delta_{\mathrm{lh}} = 0.07$). (b) and (c) are the experimental and calculated emission spectra of QD6.

δ_0 is chosen equal to 550 μeV, equally divided among the long range and short range e–h exchanges interaction. Other parameters are the same than in the previous charged exciton calculation.

4.2. Influence of the shape anisotropy

Let us consider now the influence of the electron–hole exchange interaction. We have seen in the case of non-magnetic QDs that, in first approximation, the only effect of the valence band mixing on the short range e–h exchange is to couple bright excitons states together. For magnetic QDs, bright states associated with the same Mn spin projection are thus coupled. This coupling mainly concerns the energy levels associated with Mn spin projections $\pm 1/2$ because they are only slightly split by the exciton–Mn exchange interaction. An increase of the valence band mixing will thus open a slight gap in the middle of the bright exciton fine structure (around 0.25 meV in Fig. 4(a)).

Another gap appears on the low energy side of the structure because of the hole–Mn interaction. As a matter of fact, simultaneous hole–Mn spin flips couples bright and dark states associated with consecutive Mn spin projections. The exciton–Mn exchange interaction induces an overlap of the bright and dark exciton fine structure. States coupled by h–Mn spin flips are therefore quite close to each other and an increase of the VBM, that is to say an increase of the h–Mn spin flip efficiency, will open a gap between them. This can be observed on Fig. 4(a) around -0.1 meV. Finally, one may note once again that the overall splitting of the structure decreases as the VBM increases because of the decrease of the weight of the heavy-hole in the exciton ground state.

Such coupling between bright and dark exciton is observed in the spectrum of QD6 presented in Fig. 4(b). In this QD, the valence band mixing is quite weak and the gaps induced by the e–h exchange and the h–Mn exchange can be hardly resolved in the exciton spectrum. Nevertheless, the h–Mn spin flips induced bright-dark coupling is large enough to give non-negligible oscillator strengths to the dark states. Three "dark" states are then observed in the emission spectrum. The value $\rho_s/\Delta_{\mathrm{lh}}$ can be estimated to 0.07. Using, this parameter we can calculate QD6 exciton emission spectrum. The result is plotted on Fig. 4(c). It has been shown in previous work [4] that the exciton–Mn system is partially thermalized during the exciton lifetime. This results in the increase of the intensity of the lines as their energy decreases. In the calculation we thus consider that the system has relaxed and that it is characterized by

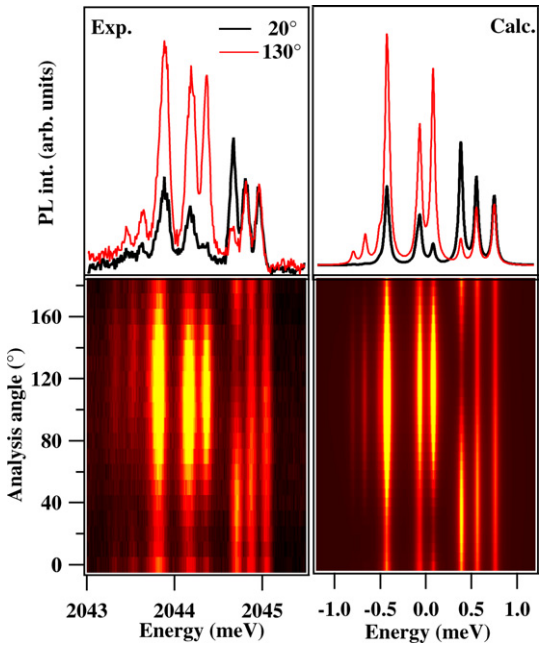

Fig. 5. Experimental and calculated polarization resolved photoluminescence of QD6. The intensity maps present the dependence of the emission on the analyzer angle. The emission spectrum are presented for orthogonal linear analyzer directions (red and black curves).

an effective spin temperature T_{eff} depending both on the phonon bath and on the hot carrier gas produced by the laser excitation. In Fig. 4(c) $T_{\text{eff}} = 15$ K. With this effective temperature, "dark" states appears in the calculated spectrum but their intensity is weaker than in the experiment. Moreover, comparing the intensities of the bright lines in the calculation and in the experiment, we note that we cannot fit the data with an effective temperature smaller than 15 K in order to increase the "dark" states intensity. These features show that we should not consider a total thermalization in the exciton–Mn system: If the spin relaxation is partially blocked, it is difficult to thermalize the system. As bright and dark excitons are created with the same generation rate, the intensities of the associated transitions can be comparable even though they have different oscillator strengths. This is particularly the case under weak excitation conditions where the influence of the hot carrier gas spin reservoir is reduced.

We finally consider the neutral exciton fine structure of a single Mn-doped QD that presents an anisotropic in-plane shape (QD6 presented in Fig. 5). Effects of the long range electron–hole exchange interaction on the emission spectrum of a single Mn-doped QD were discussed in a former letter [48]. Nevertheless, details of the polarization properties were not analyzed. Here, we detail these polarization features and show that the VBM is once again necessary to explain them. Fig. 5 presents the linear polarization dependence of the emission spectrum of QD6. The experimental spectrum show the main characteristics of a quite strong VBM as detailed in Fig. 4(a). The spectrum presents an overall linear polarization rate of about 25% orientated at $\theta_s = 110°$ from the cleaved edge of the sample and dark states appear on the low energy side of the structure. Two gaps can also be observed: One between the two first main lines and the other between the third and the fourth lines. However, if these peculiarities were only due to the combined effect of the VBM and short range e–h exchange, one could expect the third and the fourth lines to be polarized parallel and perpendicular to the strain direction (110°). It is not the case and surprisingly, the emission spectrum also presents non-orthogonal linear polarization directions.

These polarization directions are the signature of a competition between a valence band mixing and long range electron–hole exchange interaction. The calculation of the emission spectrum of QD6 (right panel of Fig. 5) gives a good agreement with the experiment using the following parameters: $I_{\text{e-Mn}} = 60$ μeV, $I_{\text{h-Mn}} = 135$ μeV, $\delta_0^{lr} = \delta_0^{sr} = 300$ μeV, $\delta_2 = 450$ μeV, $\Delta_{\text{lh}} = 30$ meV, $\rho_s/\Delta_{\text{lh}} = 0.25$ and $T_{\text{eff}} = 20$ K. The strain direction and the dot shape direction must be roughly perpendicular (80°) to fit the experiment. The main features of QD6 emission are well reproduced as presented in Fig. 5.

In anisotropic QDs, the interplay between the electron–hole and exciton–Mn exchange interactions is confirmed by magneto-optical measurements (Fig. 6). The typical Zeeman splitting of the six lines is clearly observed in the data

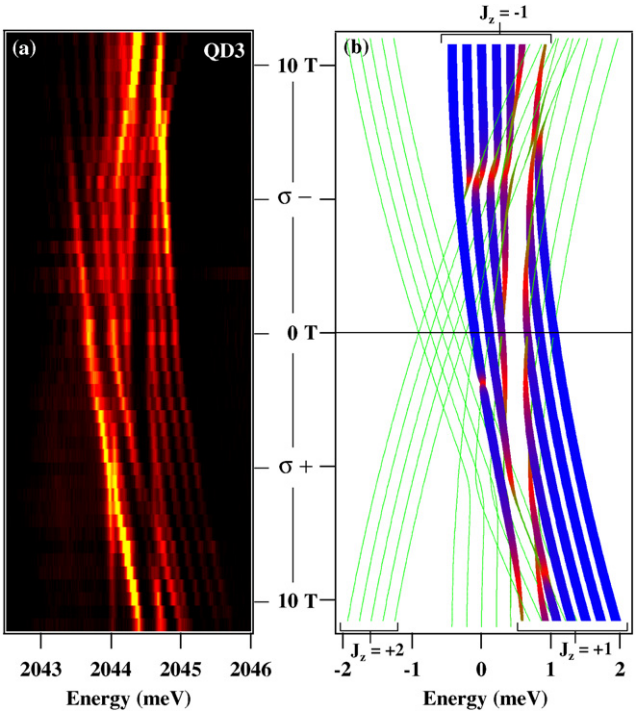

Fig. 6. (a) Intensity map of magnetic field dependence of the emission spectrum of asymmetric Mn-doped dot QD3, for circular polarization $\sigma+$ and $\sigma-$. (b) Optical transitions obtained from the diagonalization of the spin + Zeeman + diamagnetism Hamiltonian in the subspace of the 24 heavy-hole exciton and Mn spin components; Line thickness and color scale for $\sigma+$, $\sigma-$ are proportional to absolute value of the projection of the exciton state on the $J_z = +1, -1$ exciton respectively (green = low intensity, blue = high intensity). The two transitions which are forbidden at all magnetic fields ($|J_z = \pm 2, S_z = \mp 5/2\rangle$) are not plotted.

at all fields, with a strong intensity gradient at the highest fields resulting from a rather strong Mn spin polarization. For this clearly anisotropic dot, the central gap in the emission structure is maintained in both circular polarizations, with a small quadratic diamagnetic energy shift. This behavior is explained as follows: The dot anisotropy leads to successive anticrossings of the ± 1 bright exciton states associated with given Mn spin projections ($-1/2$, $-3/2$ and $-5/2$) as a function of magnetic field: As B increases, transitions associated with the $J_z = +1$ exciton shift up in energy whereas the $J_z = -1$ transitions shift down. The anisotropic part of the electron–hole exchange interaction mixes successively the $J_z = \pm 1$ exciton states associated with $S_z = -1/2$, then with $S_z = -3/2$ and finally with $S_z = -5/2$ at successively higher B. For QD3, these anticrossings are observed successively at 2.5, 7 and 11 T.

To understand fully the rich magnetic behavior of these anisotropic QDs, we calculated the optical transitions under magnetic field by diagonalizing the complete Hamiltonian of the electron–heavy hole–Mn system (including the exchange, Zeeman and diamagnetism Hamiltonians). Calculated transitions are presented in Fig. 6(b). The fitted Landé factors of the electron ($g_e = -1.1$), the hole ($g_h = 0.3$) and the Mn atom ($g_{Mn} = 2.0$), the splitting between $J_z = \pm 1$ and $J_z = \pm 2$ excitons (= 1 meV) and the diamagnetic factor ($\gamma = 2.45\ \mu eV\,T^{-2}$) agree well with previous work [30,39,4]. Parameters δ_2 and δ_{Mn} were adjusted to fit the zero field data, as explained earlier.

Comparison between calculation and data explains most of the details of the magneto-optic properties. In particular, around 7 T, the central gap is perturbed in both circular polarizations. In $\sigma-$, this is due to anticrossings induced by the mixing of $|s_e = 1/2, j_{hz} = -3/2, S_z\rangle$ states and $|-1/2, -3/2, S_z + 1\rangle$ states by the *electron*–Mn exchange, [4], i.e. corresponding to simultaneous spin-flips of electron and manganese spins. In $\sigma+$ polarization, Fig. 6(b) shows that the line of second lowest energy crosses the central gap as an essentially non-radiative transition. This implies a mixing of $|-1/2, 3/2, -3/2\rangle$ and $|-1/2, -3/2, -1/2\rangle$. This is a second order mixing involving both mixing of $|-1/2, -3/2, -1/2\rangle$ and $|1/2, -3/2, -3/2\rangle$ by the e–Mn exchange and mixing of $|-1/2, 3/2, -3/2\rangle$ and $|1/2, -3/2, -3/2\rangle$ by the anisotropic e–h exchange; that is, the e–Mn exchange induces a mixing of states mediated by the anisotropy-induced coupling.

To summarize these geometrical effects, it comes out from this study that an anisotropic stain distribution in the growth plane and a QD shape anisotropy induce a valence band mixing which strongly modifies the emission spectra of a single Mn doped QDs. The main observed effects are: (i) the appearance of anti-crossings related to possible Mn–hole spin-flips; (ii) the separation of the six lines structures into two sets of lines partially polarized; and (iii) the variation of the linear polarization directions which are no longer perpendicular for the exciton fine structure of a given QD. The last feature clearly evidences the competition between two types of anisotropy, one coming from the confinement potential (shape anisotropy) and one coming from the local strain distribution into the dot.

5. Carrier-controlled spin properties of a single magnetic atom

CdTe/ZnTe QDs are p-type modulation doped by the transfer of holes from the p-doped ZnTe substrate and from surface states that act as acceptors [41,42]. The occupation of the QDs by holes can be controlled by an external bias voltage V on an aluminium Schottky gate with respect to a back contact on the p-type substrate. The bias dependent emission of a non-magnetic QD and a Mn-doped QD is presented in Fig. 7. For increasing V, the surface level states are shifted below the ground hole level in the QDs which results in the single hole charging of the dots. The optically generated excitons then form charged excitons with the bias induced extra hole in the QD. At zero bias or negative bias, the Fermi level is above the ground state and the QDs are likely to be neutral. However, the separated capture of photo-created electron or holes can sometimes charge the dots so that weak contributions of X^+ or X^- are observed in the zero bias spectra.

At zero bias, excess electrons can also be injected in the QD using resonant optical excitation into the QD levels. Under resonant excitation (energy below the band gap of the barriers), optical transitions from delocalized valence band states to the confined electron levels will preferentially create electrons in the QD [43]: the probability to find an excess electron in the QD is increased. As presented in Fig. 7(c), the negatively charged exciton emission is then seen for some discrete excitation energies. After the recombination of the charged exciton X^-, a single hole is likely to be captured to neutralize the QD and creates a neutral exciton. This neutralization process is responsible for the simultaneous observation of charged and neutral species under resonant excitation (Fig. 7(c)).

The charge state of the dot can also be optically tuned (Fig. 7(c)). By combining a weak non-resonant excitation with the resonant one, a few carriers are created in the ZnTe barrier. They do not significantly contribute to the luminescence (lower PL spectra in Fig. 7(c)) but reduce the PL contribution of X^- in favor of the neutral species. This evolution is characteristic of a photo-depletion mechanism in modulation doped QDs [38]. High energy photoexcited e–h pairs are dissociated in the space charge region surrounding the negatively charged QDs and neutralize the QDs.

These two charge control mechanisms (bias voltage and resonant excitation combined with photo-depletion) allow one to independently probe the interaction between individual carriers (electron or hole) and an individual magnetic atom. Let us first consider the negatively charged exciton. Fig. 8(a) presents a detail of the recombination spectrum for X^- coupled with a single Mn atom obtained at zero bias under resonant excitation. Eleven emission lines are clearly observed with intensity decreasing from the outer to the inner part of the emission structure.

A simple effective spin Hamiltonian quantitatively accounts for the emission spectrum shown in Fig. 8(a). The emitting state in the X^- transition has two conduction band (CB) electrons and one hole coupled to the Mn. The effect of the two spin-paired electrons on the Mn is strictly zero. Thereby, the spin structure of the X^- state is governed by the interaction of the hole with the Mn. Based upon the results presented in Section 3, we propose the following Hamiltonian:

$$\mathcal{H}_{\mathrm{h-Mn}} = I_{\mathrm{h}}\left(S_z j_z + \frac{\epsilon}{2}(j_- S_+ + j_+ S_-)\right) \tag{8}$$

where $\vec{S}$ is the Mn spin operator and $\vec{j}$ acts on the hole lowest energy doublet. The first term is the spin conserving or Ising exchange whereas the second is only possible if there are some heavy-light hole mixing [44]. From our measurements we find that ϵ is small and, in a first stage, we neglect it. Later we will show its influence. The twelve eigenstates of $\mathcal{H}_{\mathrm{h-Mn}}$ with $\epsilon = 0$ are organized as six doublets (Fig. 8(b)) with well defined S_z and j_z (Mn and hole spin along the z axis). We label these states as $|S_z, j_z\rangle$. Recombination of one of the CB electrons with the hole of the X^- state leaves a final state with a single CB electron coupled to the Mn. The spin Hamiltonian of this system is the ferromagnetic Heisenberg model, $\mathcal{H}_{\mathrm{e-Mn}} = -I_{\mathrm{e}}\vec{S}\cdot\vec{\sigma}_{\mathrm{e}}$. The twelve eigenstates of the Mn–electron complex are

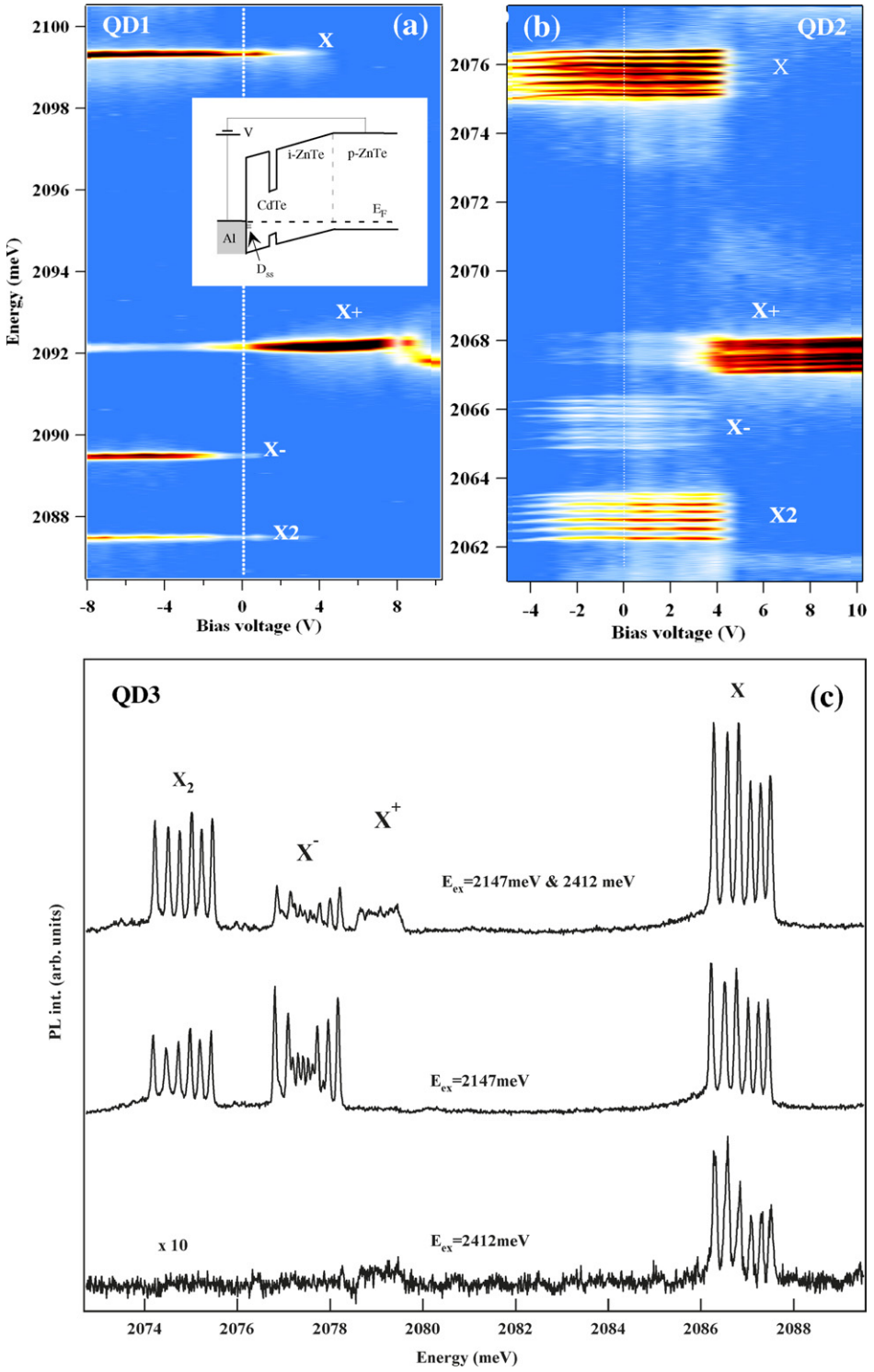

Fig. 7. Color-scale plot of the photoluminescence intensity of a non-magnetic QD (a) and a single Mn-doped QD (b) in a Schottky structure as a function of emission energy and bias voltage. The series of emission lines can be assigned to QD s-shell transitions, namely the recombination of the neutral exciton (X), biexciton (X^2), positively charged exciton (X^+) and negatively charged exciton (X^-). Detail of the PL of a single Mn-doped QD under resonant excitation ($E_{ex} = 2147$ meV), non-resonant excitation ($E_{ex} = 2412$ meV) and both resonant and non-resonant excitation.

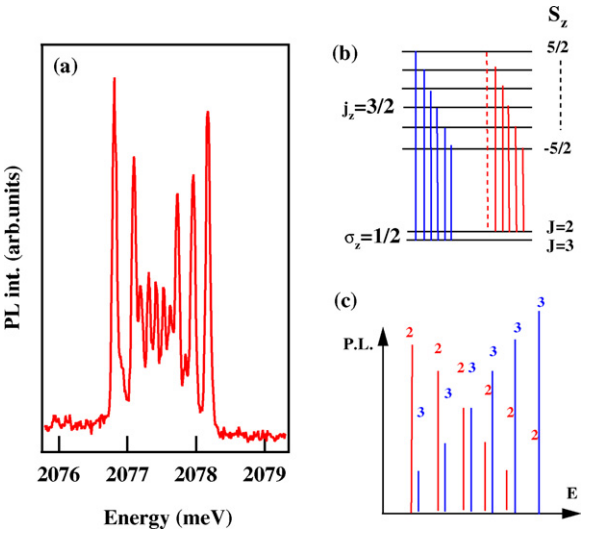

Fig. 8. (a) Detail of the unpolarized emission spectrum of a negatively charged exciton (X^-) coupled with a Mn atom. (b) Scheme of the $\sigma+$ optical transitions of (X^-, Mn) and their respective PL intensity distribution (c).

splitted into a ground state septuplet (total spin $J = 3$) and a five-fold degenerate manifold with $J = 2$. We label them all as $|J, J_z\rangle$.

Thus, for each of the six doublets of X^- there are two possible final states after annihilation of an e–h pair, with either $J = 2$ or $J = 3$. From this consideration alone, we would expect twelve spectrally resolved lines. Their weight is given by both optical and spin conservation rules. Since electrons and holes reside in s and p bands respectively, the $\Delta L = 1$ optical selection rule is immediately satisfied. The polarization of the photon imposes an additional selection rule on ΔM which is accounted for by the spin of the electron and hole. The Mn spin is not affected by the transition.

The weight of optical transitions between the initial state $|i\rangle = (\uparrow, \downarrow)_e \times |S_z, j_z\rangle$ and the final state $|f\rangle = |J, J_z\rangle$ is proportional to: $|\langle f| \sum_\sigma P(\sigma, j_z) c_\sigma d_{j_z} |i\rangle|^2$ where c_σ annihilates a CB electron with spin σ, and d_{j_z} annihilates a VB hole with angular momentum j_z. Here $P(\sigma, j_z)$ is given by the polarization selection rule.

Let us consider, for instance, $\sigma+$ recombination transitions where the $(\downarrow_e, \Uparrow_h)$ e–h pair is annihilated. Each of the six doublets, characterized by their Mn spin projection S_z, can be an initial state. After the electron–hole annihilation, the resulting state is $|S_z, \uparrow_e\rangle$ which, in general, is not an eigenstate of $\mathcal{H}_{e,Mn}$. The intensity of the optical transition to a given final state $|J, J_z\rangle$ is proportional to the overlap $\langle J, J_z | S_z, \uparrow_e\rangle$, which is nothing but a Clebsh Gordan coefficient. The highest energy transition, with $\sigma+$ polarization, would correspond to the initial state $(\uparrow, \downarrow)_e \times |+5/2, \Uparrow_h\rangle$ and a low energy final state $|J = 3, J_z\rangle$. After the photon emission, the state of the system is $|S_z = +5/2, \uparrow_e\rangle$ which is identical to $|J = 3, J_Z = +3\rangle$ and thereby gives the highest optical weight (Fig. 8(b)). In contrast, emission from that initial state to $|J = 2, J_z\rangle$ is forbidden. The other five doublets have optical weights lying between $1/6$ and $5/6$ with both $|J = 2, J_z\rangle$ and $|J = 3, J_z\rangle$ final states. Thereby, the number of spectrally resolved lines in this model is 11.

The relative weight of the emission lines is accounted for by the model. According to the final state, the transitions belong to either the $J = 2$ or the $J = 3$ series. As the initial S_z decreases, the overlap of $|\uparrow_e S_z\rangle$ to the $J = 3$ ($J = 2$) states decreases (increases). As presented in Fig. 8(c), the PL of X^- can be seen as a superposition of two substructures: six lines with intensities increasing with their energy position (transitions to $J = 3$ states) and five lines with intensities decreasing with increasing their energy position (transitions to $J = 2$ states).

Reversing the role of the initial and final states, and neglecting the small coupling of two holes to the Mn spin [50], this model should account for the emission from X^+ states. Actually, different energy splittings are observed for the different excitonic species in the same QD. For instance, in QD3 (Fig. 7(c)) one measured $\Delta E_X = 1.23$ meV, $\Delta E_{X-} = 1.36$ meV and $\Delta E_{X+} = 0.95$ meV. The energy splitting is mostly due to the Mn–hole exchange coupling, which in turn is inversely proportional to the volume of the hole wave function. The difference between ΔE_{X+} and ΔE_{X-} indicates that a significant fraction of the confinement of the hole comes from the Coulomb attraction of the two electrons in the initial state of the X^- emission. In contrast, in the final state of the X^+ emission, there is no electron to attract the hole, resulting in a spread of the hole wave function and a smaller exchange energy. This

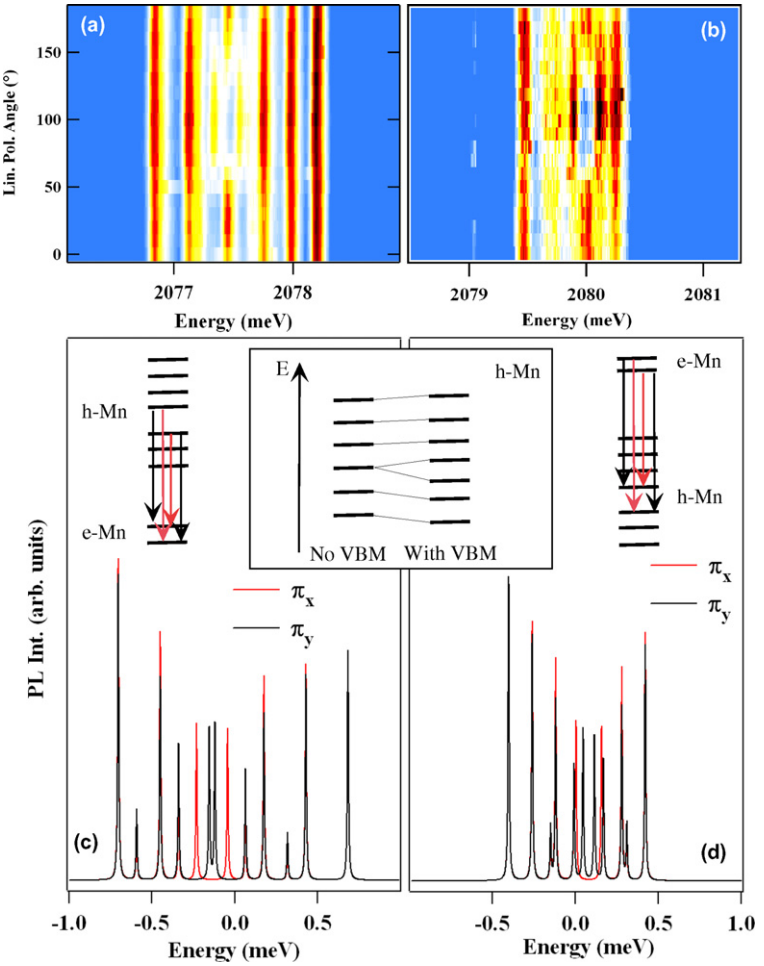

Fig. 9. Color scale plot of the dependence of the PL of (X^-, Mn) (a) and (X^+, Mn) (b) on the direction of a linear analyzer, in the same QD. Three lines in the center of the structure are linearly polarized. (c) and (d): calculated linearly polarized PL spectra of (X^-, Mn) and (X^+, Mn) with exchange integrals I_e and I_h chosen to reproduce the overall splitting for X^+ and X^- presented in (a) and (b). Transitions are arbitrarily broadened by 10 μeV. The schemes in (c) and (d) show energy levels involved in (X^-, Mn) and (X^+, Mn) recombination with valence band mixing. The central inset presents the energy level scheme of the h–Mn system without and with valence band mixing (VBM).

difference appears directly in the emission structure shown in Fig. 7, where the peak structure of X^+ is not well resolved.

In Fig. 9(a) we show the intensity of X^- emission as a function of the direction of a linear analyzer. It is apparent that the central lines are linearly polarized. This polarization can only be understood if we allow for some spin-flip interaction between the Mn and the hole (second term in Eq. (8)). Provided that $\epsilon \ll 1$, the effect of this interaction is small both on the wave function and on the degeneracy of all the doublets except the third, which is split, as illustrated in the inset of Fig. 9. The split states are the bonding and antibonding combinations of $|S_z = -1/2, \Uparrow_h\rangle$ and $|S_z = +1/2, \Downarrow_h\rangle$. These states are coupled, via linearly polarized photons, to the $|2, 0\rangle$ and $|3, 0\rangle$ e–Mn complex and four linearly polarized lines should be observed on the emission spectra as shown in the insets of Fig. 9(c) and (d). Polarization directions are controlled by the distribution of strains through the Bir–Pikus Hamiltonian [44,51].

We can obtain numerical values of I_h, I_e and ϵ for the charged excitons comparing the transition probabilities calculated with model (8) (Fig. 9(c)) to the experimental data. The electron–Mn exchange integral I_e is deduced from magneto-optics measurements on the neutral exciton [4]. I_h, the hole–Mn exchange integral, is then chosen to reproduce the overall splitting of the two charged species emission structure. There is a good agreement between the experimental data (QD3 in Fig. 7(c)) and our model with $I_e = 40$ μeV, $I_h(X) = 150$ μeV, $I_h(X^+) = 95$ μeV and $I_h(X^-) = 170$ μeV. The different values of I_h directly reflect the expected variation of the confinement of the hole. The

main characteristics of the emission spectra are well reproduced, namely the number of emission lines, their intensity distribution and the linear polarization structure, with a slight valence band mixing coefficient $\epsilon = 0.05$. This small value of the valence band mixing coefficient shows that hole–Mn exchange interaction remains highly anisotropic.

6. Conclusion

Let us recall that the precise control of electronic spins in semiconductors is a very active field nowadays, the so-called spintronics, which needs, besides the potential applications, to have a deep insight of the effects which combine manipulation of charges and manipulation of spins. In this large field of activity, the development of techniques for the optical control of single spins in the solid state is motivated by the possibility of using single spins embedded in nano-structures for the implementation of quantum information processing devices. These devices will be required to detect and manipulate individual spins and to make them interact with the semiconductor carriers. However, in such nanometer size system, it is important to tune independently the quantum dot charge states and the magnetic doping in order to elucidate the interactions with the different charge carriers.

Quantum dots made of a II-VI semiconductor (such as CdTe) in which Manganese atoms randomly substitute Cadmium (Mn in II-VI's is an isoelectronic impurity, i.e., it is not electrically active) allow one to tune properly the various configurations. In particular, we can study the case of a single Mn atom interacting with an excess of one hole, which is the expected configuration in the world-wide developed III-V semiconductor quantum dots.

We have shown that the injection of a controlled number of carriers in an individual II-VI QD allows us to control the spin splitting of a single magnetic ion. The exchange interaction with a single carrier acts as an effective local magnetic field that split the Mn levels in zero-applied magnetic field. We have fabricated a device with electrically tunable magnetic properties, in analogy with two dimensional DMS based electrically active heterostructures [8–10], but scaling the number of controlled magnetic atoms down to one and the size of the active region down to a few nanometers. Micro-photoluminescence experiments have allowed us to identify three magnetically different ground states corresponding to three charge states ($\pm$1e and 0) and to measure the exchange interaction of both a single electron and a single hole with a single magnetic atom. The final state of (X^+, Mn) transition (1h, 1Mn) is non-degenerate in the absence of external magnetic field. This splitting of the different spin configurations should efficiently increase the spin relaxation time of both Mn and holes.

The observation of an individual spin in a quantum dot opens new possibilities in information storage. The spin of an isolated Mn atom should present a relaxation time in the millisecond range. This property could be exploited to store digital information on a single atom. The device presented here is a first step towards the development of new memories in which an information digit would be stored on the spin state of an individual atom.

Acknowledgements

The authors thank J. Fernandez-Rossier for fruitful discussions. This work was partly supported by the French-ANR contracts MOMES and CoSin.

References

[1] H.C. Manoharan, C.P. Lutz, D.M. Eigler, Nature 403 (2000) 512.
[2] P. Gambardella, S. Rusponi, M. Veronese, S.S. Dhesi, C. Grazioli, A. Dallmeyer, I. Cabria, R. Zeller, P.H. Dederichs, K. Kern, C. Carbone, H. Brune, Science 300 (2003) 1130.
[3] A.M. Yakunin, A.Yu. Silov, P.M. Koenraad, J.-M. Tang, M.E. Flatte, W.V. Roy, J.D. Boeck, J.H. Wolter, Phys. Rev. Lett. 92 (2004) 216806.
[4] L. Besombes, Y. Leger, L. Maingault, D. Ferrand, H. Mariette, J. Cibert, Phys. Rev. Lett. 93 (2004) 207403.
[5] A. Kudelski, A. Lemaitre, A. Miard, P. Voisin, T.C.M. Graham, R.J. Warburton, O. Krebs, Phys. Rev. Lett. 99 (2007) 247209.
[6] A.J. Heinrich, A. Gupta, C.P. Lutz, D.M. Eigler, Science 306 (2004) 466–469.
[7] F. Jelezko, T. Gaebel, I. Popa, A. Gruber, J. Wrachtrup, Phys. Rev. Lett. 92 (2004) 076401.
[8] H. Ohno, D. Chiba, F. Matsukura, T. Omiya, E. Abe, T. Dietl, Y. Ohno, K. Ohtani, Nature 408 (2000) 944.
[9] H. Boukari, P. Kossacki, M. Bertolini, D. Ferrand, J. Cibert, S. Tatarenko, A. Wasiela, J.A. Gaj, T. Dietl, Phys. Rev. Lett. 88 (2002) 207204.
[10] D. Chiba, M. Yamanouchi, F. Matsukura, H. Ohno, Science 301 (2003) 943.
[11] Al.L. Efros, E.I. Rashba, M. Rosen, Phys. Rev. Lett. 87 (2001) 206601.
[12] A.O. Govorov, A.V. Kalameitsev, Phys. Rev. B 71 (2005) 035338;
A.O. Govorov, Phys. Rev. B 72 (2005) 075359.

[13] J.I. Climente, M. Korkusinski, P. Hawrylak, J. Planelles, Phys. Rev. B 71 (2005) 125321;
F. Qu, P. Hawrylak, Phys. Rev. Lett. 95 (2005) 217206;
F. Qu, P. Hawrylak, Phys. Rev. Lett. 96 (2006) 157201.
[14] J. Fernandez-Rossier, L. Brey, Phys. Rev. Lett. 93 (2004) 117201.
[15] A.O. Govorov, Phys. Rev. B 72 (2005) 075358.
[16] F. Qu, P. Hawrylak, Phys. Rev. Lett. 96 (2006) 157201.
[17] A.V. Chernenko, P.S. Dorozhkin, V.D. Kulakovskii, A.S. Brichkin, S.V. Ivanov, A.A. Toropov, Phys. Rev. B 72 (2005) 045302.
[18] A.A. Maksimov, G. Bacher, A. McDonald, V.D. Kulakovskii, A. Forchel, C.R. Becker, G. Landwehr, L.W. Molenkamp, Phys. Rev. B 62 (2000) R7767.
[19] J. Seufert, G. Bacher, M. Scheibner, A. Forchel, S. Lee, M. Dobrowolska, J.K. Furdyna, Phys. Rev. Lett. 88 (2002) 027402.
[20] G. Mackh, W. Ossau, D.R. Yakovlev, A. Waag, G. Landwehr, R. Hellmann, E.O. Gobel, Phys. Rev. B 49 (1994) 10248.
[21] D.R. Yakovlev, K.V. Kavokin, I.A. Merkulov, G. Mackh, W. Ossau, R. Hellmann, E.O. Gobel, A. Waag, G. Landwehr, Phys. Rev. B 56 (1997) 9782.
[22] P.S. Dorozhkin, A.V. Chernenko, V.D. Kulakovskii, A.S. Brichkin, A.A. Maksimov, H. Schoemig, G. Bacher, A. Forchel, S. Lee, M. Dobrowolska, J.K. Furdyna, Phys. Rev. B 68 (2003) 195313.
[23] A. Hundt, J. Puls, H. Henneberger, Phys. Rev. B 69 (2004) 121309.
[24] G. Bacher, A.A. Maksimov, H. Schömig, V.D. Kulakovskii, M.K. Welsh, A. Forchel, P.S. Dorozhkin, A.V. Chernenko, S. Lee, M. Dobrowolska, J.K. Furdyna, Phys. Rev. Lett. 89 (2002) 127201.
[25] D.J. Norris, Nan Yao, F.T. Charnock, T.A. Kennedy, Nano Lett. 1 (2001) 3.
[26] S.C. Erwin, L. Zu, M.I. Haftel, A.L. Efros, T.A. Kennedy, D.J. Norris, Nature 436 (2005) 91.
[27] A.K. Bhattacharjee, J. Perez-Conde, Phys. Rev. B 68 (2003) 045303.
[28] P.I. Archer, S.A. Santangelo, D.R. Gamelin, Nano Lett. 7 (2007) 1037.
[29] S. Mackowski, T. Gurung, H.E. Jackson, L.M. Smith, G. Karczewski, J. Kossut, Appl. Phys. Lett. 87 (2005) 072502.
[30] J.K. Furdyna, J. Appl. Phys. 64 (1998) R29.
[31] J.K. Furdyna, J. Kossut (Eds.), Semiconductors and Semimetals, vol. 25, Academic, Boston, 1988.
[32] J. Schneider, U. Kaufmann, W. Wilkening, M. Baeumler, F. Kohl, Phys. Rev. Lett. 59 (1987) 240.
[33] M. Linnarsson, E. Janzén, B. Monemar, M. Kleverman, A. Thilderkvist, Phys. Rev. B 55 (1997) 6938.
[34] L. Maingault, L. Besombes, Y. Leger, C. Bougerol, H. Mariette, Appl. Phys. Lett. 89 (2006) 193109.
[35] J.A. Gaj, R. Planel, G. Fishman, Solid State Commun. 29 (1979) 435.
[36] A. Twardowski, P. Swiderski, M. von Ortenberg, R. Pauthenet, Solid State Commun. 50 (1984) 509.
[37] A.O. Govorov, Phys. Rev. B 70 (2004) 035321.
[38] A. Hartmann, Y. Ducommun, E. Kapon, U. Hohenester, E. Molinari, Phys. Rev. Lett. 84 (2000) 5648.
[39] L. Besombes, K. Kheng, D. Martrou, Phys. Rev. Lett. 85 (2000) 425;
L. Besombes, K. Kheng, D. Martrou, J. Crystal Growth 214 (2000) 742.
[40] I.A. Merkulov, D.R. Yakovlev, A. Keller, W. Ossau, J. Geurts, A. Waag, G. Landwehr, G. Karczewski, T. Wojtowicz, J. Kossut, Phys. Rev. Lett. 83 (1999) 1431.
[41] W. Maslana, P. Kossacki, M. Bertolini, H. Boukari, D. Ferrand, S. Tatarenko, J. Cibert, J.A. Gaj, Appl. Phys. Lett. 82 (2003) 1875.
[42] S. Bhunia, D.N. Bose, J. Appl. Phys. 87 (2000) 2931.
[43] A. Vasanelly, R. Ferreira, G. Bastard, Phys. Rev. Lett. 89 (2002) 216804.
[44] A.V. Koudinov, I.A. Akimov, Yu.G. Kusrayev, F. Henneberger, Phys. Rev. B 70 (2004) 241305.
[45] Y. Léger, L. Besombes, L. Maingault, D. Ferrand, H. Mariette, Phys. Rev. B 72 (2005) 241309.
[46] Y. Léger, L. Besombes, J. Fernández-Rossier, L. Maingault, H. Mariette, Phys. Rev. Lett. 97 (2006) 107401.
[47] Y. Léger, L. Besombes, L. Maingault, H. Mariette, Phys. Rev. B 76 (2007) 045331.
[48] Y. Léger, L. Besombes, L. Maingault, D. Ferrand, H. Mariette, Phys. Rev. Lett. 95 (2005) 047403.
[49] J. Allègre, B. Gil, J. Calatayud, H. Mathieu, J. Crys. Growth 101 (1990) 603.
[50] L. Besombes, Y. Leger, L. Maingault, D. Ferrand, H. Mariette, J. Cibert, Phys. Rev. B 71 (2005) 161307.
[51] M. Tadic, F.M. Peeters, K.L. Janssens, Phys. Rev. B 65 (2002) 165333.
[52] U. Bockelmann, G. Bastard, Phys. Rev. B 45 (1992) 1688.
[53] T. Tanaka, J. Singh, Y. Arakawa, P. Bhattacharya, Appl. Phys. Lett. 62 (1993) 756.
[54] S. Cortez, O. Krebs, P. Voisin, J. Vac. Sci. Technol. B 18 (2000) 2232.